Fracture Mechanics of Concrete Structures
Proceedings FRAMCOS-3
AEDIFICATIO Publishers, D-79104 Freiburg, Germany

MODELLING OF CRACK PROPAGATION WITH EMBEDDED DISCONTINUITY ELEMENTS

L.J. Sluys,
Koiter Institute Delft / Delft University of Technology, the Netherlands

Abstract

A modelling in which the crack is incorporated in the shape functions of the finite element formulation is used in this paper. The crack is represented by a discontinuous function of the displacement gradients, which acts as an additional localized mode with a length scale parameter that is independent of the element size. A predefinition of the direction of the crack is not necessary and the failure zone can be described with a relatively small number of finite elements. This embedded crack/discontinuity model is compared with the widely used fracture energy model.
Keywords: Embedded discontinuity concept, fixed/rotating models.

1 Introduction

For large scale and three-dimensional (3D) computations of fracture a modelling of the failure zone with embedded discontinuities can be highly effective. The crack is regarded as a jump in the displacements (Ortiz et al., 1987; Simo et al., 1993; Armero and Garikipati, 1995; Larsson et al., 1995; Lotfi and Shing, 1995) or the displacement gradients (Belytschko et al., 1988; Sluys and Berends, 1998). These jump functions are so-called additional localization modes which can be added to the standard shape functions of the finite element. The discontinuous modelling limits the number of finite elements that is needed to describe the crack in comparison with

higher-order continua such as gradient models (Aifantis, 1984; de Borst et al., 1992) and nonlocal models (Pijaudier-Cabot and Bažant, 1987), which is extremely important for large scale and 3D calculations of crack propagation.

The model with a discontinuity in the strain field will be explained for 1D, 2D and 3D stress situations. Simple elements are used, namely for 1D a linear truss, for 2D a constant strain triangle and for 3D a 4-noded tetrahedral element. These are the underlying elements to which the localized modes are added. In the discontinuity element a length scale parameter is introduced which is a material parameter and can be related to the size of the fracture process zone. This solves the mesh-size dependence problem as present when a standard crack model is used. The amplitudes of the localized mode are obtained from the traction continuity condition that must be satisfied over the discontinuity line and the assumption of compatibity of deformation (related to satisfaction of the patch test). The amplitudes are additional degrees-of-freedom that are solved at integration point level. A predefinition of the direction of the crack is not necessary and the failure zone can be described with a relatively small number of finite elements. The model can be combined with different sets of constitutive equations (cracking, damage, plasticity).

1D, 2D and 3D examples of mode-I failure problems will be analyzed. Two important issues will be discussed in the paper. Firstly, the problem of mesh locking which appears in this discontinuity concept when the discontinuity plane is fixed after initiation of the crack. Secondly, crack propagation in structured and unstructured meshes will be analyzed to assess the the performance of the model with respect to mesh-orientation sensitivity. Similarities and differences between the model presented here and the fracture energy model are explained.

2 Kinematics of discontinuous failure

In the approach proposed in this paper a discontinuity of velocity gradient at the edges of the localization zone is assumed (see Figure 1). The displacements and the velocities in the localized area are still continuous. For a jump in velocity gradient $\dot{u}_{i,j}$ between cracked and non-cracked material we define

$$[\![\dot{u}_{i,j}]\!] = \bar{\alpha} m_i n_j \ , \tag{1}$$

in which the vector $\mathbf{n}$ is the normal to the discontinuity plane, the vector $\mathbf{m}$ defines the nature of the discontinuity and $\bar{\alpha}$ is the jump coefficient. For a pure mode-I failure plane $\mathbf{m}$ is aligned with $\mathbf{n}$ and $\mathbf{n}^T\mathbf{m} = 1$, on the other hand for a pure mode-II failure $\mathbf{m}$ is perpendicular to $\mathbf{n}$ and $\mathbf{n}^T\mathbf{m} = 0$. Fur-

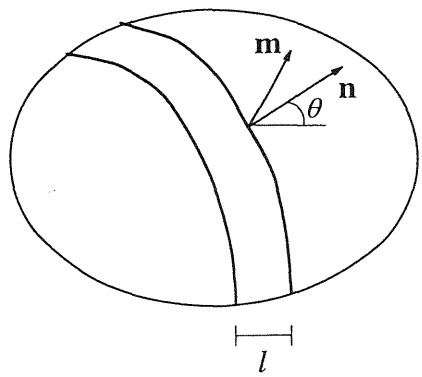

Fig. 1. Definition of localized band.

thermore in Figure 1 the angle θ determines the orientation of the discontinuity plane and the parameter l plays the role of the localization band width. This parameter appears as an independent material parameter and is not set by the finite element size. From the jump of velocity gradient we can define the jump in strain rate according to

$$[\![\dot{\varepsilon}_{ij}]\!] = \frac{\bar{\alpha}}{2}(m_i n_j + m_j n_i) \tag{2}$$

or

$$[\![\dot{\boldsymbol{\varepsilon}}]\!] = \bar{\alpha}\mathbf{q}\,. \tag{3}$$

At both edges of the localization band we distinguish jumps in the displacement gradient. We define two jump coefficients $\bar{\alpha}_1$ and $\bar{\alpha}_2$ that determine the additional strain field of the localized mode. The jump $\bar{\alpha}_1$ represents the decrease in strain in the elastic area and $\bar{\alpha}_2$ denotes the increase of strain in the inelastic area, both with respect to a formulation without additional jump functions. We can now derive expressions for the strain rate outside the band $\dot{\boldsymbol{\varepsilon}}_1$ and inside the band $\dot{\boldsymbol{\varepsilon}}_2$ according to

$$\dot{\boldsymbol{\varepsilon}}_1 = \mathbf{L}\dot{\mathbf{u}} - \bar{\alpha}_1\mathbf{q} \tag{4}$$

$$\dot{\boldsymbol{\varepsilon}}_2 = \mathbf{L}\dot{\mathbf{u}} + \bar{\alpha}_2\mathbf{q}\,, \tag{5}$$

in which $\mathbf{L}$ is the differential operator matrix. In a finite element set-up we discretize the continuous displacement field $\mathbf{u}$ by

$$\dot{\mathbf{u}} = \mathbf{H}\dot{\mathbf{a}}\,, \tag{6}$$

in which the matrix $\mathbf{H}$ contains the interpolation polynomials and $\dot{\mathbf{a}}$ are the nodal velocities. If we substitute eq.(6) and introduce the strain-nodal displacement matrix $\mathbf{B} = \mathbf{LH}$ eqs.(4) and (5) become

$$\dot{\varepsilon}_1 = \mathbf{B}\dot{\mathbf{a}} - \bar{\alpha}_1 \mathbf{q} \tag{7}$$

$$\dot{\varepsilon}_2 = \mathbf{B}\dot{\mathbf{a}} + \bar{\alpha}_2 \mathbf{q} \,. \tag{8}$$

For convenience we can rewrite eqs.(7) and (8) by multiplication of the additional strain field by the scalar quantity $\mathbf{q}^{\mathrm{T}}\mathbf{B}\dot{\mathbf{a}}$ and obtain

$$\dot{\varepsilon}_1 = \bar{\mathbf{B}}_1 \dot{\mathbf{a}} \tag{9}$$

and

$$\dot{\varepsilon}_2 = \bar{\mathbf{B}}_2 \dot{\mathbf{a}} \tag{10}$$

where

$$\bar{\mathbf{B}}_1 = [\mathbf{I} - \alpha_1 \mathbf{q}\mathbf{q}^{\mathrm{T}}]\,\mathbf{B} \tag{11}$$

$$\bar{\mathbf{B}}_2 = [\mathbf{I} + \alpha_2 \mathbf{q}\mathbf{q}^{\mathrm{T}}]\,\mathbf{B} \tag{12}$$

with $\bar{\alpha}_1 = \alpha_1 \mathbf{q}^{\mathrm{T}}\mathbf{B}\dot{\mathbf{a}}$ and $\bar{\alpha}_2 = \alpha_2 \mathbf{q}^{\mathrm{T}}\mathbf{B}\dot{\mathbf{a}}$. In the model the unknowns $\mathbf{m}$ and α_1 and α_2 need to be determined.

3 Finite element discretization

To enforce equilibrium we assume at the end of the time or loading step

$$\mathbf{L}^{\mathrm{T}} \boldsymbol{\sigma}^{t+\Delta t} = \mathbf{0} \,. \tag{13}$$

The weak form of eq.(13) for an element with an elastic zone Ω_1 and a localized zone Ω_2 ($\Omega = \Omega_1 + \Omega_2$ is the total area of an element) is as follows

$$\int_{\Omega_1} \delta\dot{\mathbf{u}}^{\mathrm{T}} [\mathbf{L}^{\mathrm{T}} \sigma_1^{t+\Delta t}]\, \mathrm{d}\Omega_1 + \int_{\Omega_2} \delta\dot{\mathbf{u}}^{\mathrm{T}} [\mathbf{L}^{\mathrm{T}} \sigma_2^{t+\Delta t}]\, \mathrm{d}\Omega_2 = 0 \,, \tag{14}$$

or invoking the divergence theorem

$$\int_{\Omega_1} \delta\dot{\varepsilon}_1{}^{\mathrm{T}} \boldsymbol{\sigma}_1^{t+\Delta t}\, \mathrm{d}\Omega_1 + \int_{\Omega_2} \delta\dot{\varepsilon}_2{}^{\mathrm{T}} \boldsymbol{\sigma}_2^{t+\Delta t}\, \mathrm{d}\Omega_2 - \int_S \delta\dot{\mathbf{u}}^{\mathrm{T}} \mathbf{p}^{t+\Delta t}\, \mathrm{d}S = 0 \,, \tag{15}$$

in which $\mathbf{p}$ are the tractions at boundary S. For an incremental-iterative procedure the stress at time $t + \Delta t$ in both elastic and localized part is decomposed into the stress at time t and the stress increment

$$\boldsymbol{\sigma}_{1,2}^{t+\Delta t} = \boldsymbol{\sigma}_{1,2}^{t} + \Delta\boldsymbol{\sigma}_{1,2} \,, \tag{16}$$

which can be substituted into eq.(15)

$$\int_{\Omega_1} \delta\dot{\varepsilon}_1{}^{\mathrm{T}} \Delta\boldsymbol{\sigma}_1\, \mathrm{d}\Omega_1 + \int_{\Omega_2} \delta\dot{\varepsilon}_2{}^{\mathrm{T}} \Delta\boldsymbol{\sigma}_2\, \mathrm{d}\Omega_2 =$$

$$\int_S \delta\dot{\mathbf{u}}^{\mathrm{T}} \mathbf{p}^{t+\Delta t}\, \mathrm{d}S - \int_{\Omega_1} \delta\dot{\varepsilon}_1{}^{\mathrm{T}} \boldsymbol{\sigma}_1^{t}\, \mathrm{d}\Omega_1 - \int_{\Omega_2} \delta\dot{\varepsilon}_2{}^{\mathrm{T}} \boldsymbol{\sigma}_2^{t}\, \mathrm{d}\Omega_2 \,. \tag{17}$$

The constitutive equations in linearized format for the elastic part read

$$\Delta\sigma_1 = \mathbf{D}^e \Delta\varepsilon_1 \tag{18}$$

with matrix $\mathbf{D}^e$ containing the elastic stiffness moduli, and for the localized part

$$\Delta\sigma_2 = \mathbf{D}^i \Delta\varepsilon_2 \tag{19}$$

with $\mathbf{D}^i$ the matrix with the tangential stiffnes moduli. Substitution of eqs.(18) and (19) into eq.(17) results in

$$\int_{\Omega_1} \delta\dot{\varepsilon}_1{}^{\mathrm{T}} \mathbf{D}^e \Delta\varepsilon_1 \, \mathrm{d}\Omega_1 + \int_{\Omega_2} \delta\dot{\varepsilon}_2{}^{\mathrm{T}} \mathbf{D}^i \Delta\varepsilon_2 \, \mathrm{d}\Omega_2 =$$

$$\int_S \delta\dot{\mathbf{u}}^{\mathrm{T}} \mathbf{p}^{t+\Delta t} \, \mathrm{d}S - \int_{\Omega_1} \delta\dot{\varepsilon}_1{}^{\mathrm{T}} \sigma_1^t \, \mathrm{d}\Omega_1 - \int_{\Omega_2} \delta\dot{\varepsilon}_2{}^{\mathrm{T}} \sigma_2^t \, \mathrm{d}\Omega_2 \,. \tag{20}$$

Now for ε_1 and ε_2 the enhanced strain fields according to eqs.(9) and (10) can be substituted. Together with eq.(6) and the assumption that the equation must hold for any admissible field $\delta\dot{\mathbf{a}}$ transforms eq.(20) in

$$\mathbf{K}\Delta\mathbf{a} = \mathbf{f}_e - \mathbf{f}_i \,, \tag{21}$$

in which

$$\mathbf{K} = \int_{\Omega_1} \bar{\mathbf{B}}_1{}^{\mathrm{T}} \mathbf{D}^e \bar{\mathbf{B}}_1 \, \mathrm{d}\Omega_1 + \int_{\Omega_2} \bar{\mathbf{B}}_2{}^{\mathrm{T}} \mathbf{D}^i \bar{\mathbf{B}}_2 \, \mathrm{d}\Omega_2 \,, \tag{22}$$

$$\mathbf{f}_e = \int_S \mathbf{H}^{\mathrm{T}} \mathbf{p}^{t+\Delta t} \, \mathrm{d}S \,, \tag{23}$$

$$\mathbf{f}_i = \int_{\Omega_1} \bar{\mathbf{B}}_1{}^{\mathrm{T}} \sigma_1^t \, \mathrm{d}\Omega_1 + \int_{\Omega_2} \bar{\mathbf{B}}_2{}^{\mathrm{T}} \sigma_2^t \, \mathrm{d}\Omega_2 \,. \tag{24}$$

The calculation of Ω_1 and Ω_2 is of crucial importance for the success of the method.

4 1D element

For the one-dimensional case the normal to the crack plane $\mathbf{n}$ is aligned with vector $\mathbf{m}$, i.e. $\mathbf{n}^{\mathrm{T}} = \mathbf{m}^{\mathrm{T}} = (1, 0)^{\mathrm{T}}$. Hence, after the addition of the localized mode the incremental strains outside and inside the localization zone according to eqs.(7) and (8) reduce to

$$\Delta\varepsilon_1 = (1 - \alpha_1)\,\mathbf{B}\Delta\mathbf{a} \tag{25}$$

and

$$\Delta\varepsilon_2 = (1 + \alpha_2)\,\mathbf{B}\Delta\mathbf{a} \,, \tag{26}$$

with $\mathbf{B} = (1/d)[-1, 1]$ for a two-noded truss element and with α_1 and α_2 the

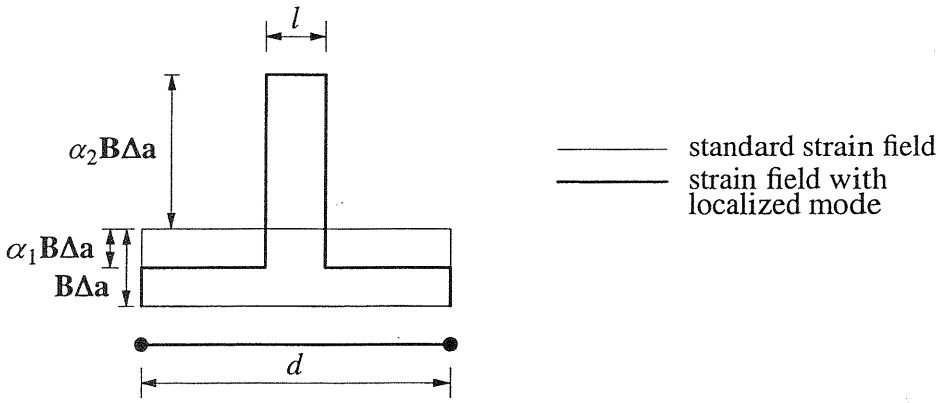

Fig. 2. Linear truss element with additional localized mode.

amplitudes of the localized mode as given in Figure 2. The length of the truss element is d and l is the localization band width as explained in section 2. The amplitudes α_1 and α_2 can be determined from the assumptions of compatibility of deformation and traction continuity over the discontinuity lines (see also Belytschko et al. (1988)). The addition of the localized mode to the standard shape functions may not lead to additional nodal displacements. For the two-noded truss element this condition results in

$$d\,\mathbf{B}\Delta\mathbf{a} = (d - l)\Delta\varepsilon_1 + l\Delta\varepsilon_2 \,. \tag{27}$$

which after use of eqs.(25) and (26) leads to

$$\alpha_1 = \left(\frac{l}{d-l}\right)\alpha_2 \,. \tag{28}$$

The assumption of traction continuity reads

$$\Delta\sigma_1 = \Delta\sigma_2 \,. \tag{29}$$

For the elastic part we have

$$\Delta\sigma_1 = E\Delta\varepsilon_1 \,, \tag{30}$$

with E the Young's modulus, and for the localized part of the finite element the incremental stress has an elastic component $\Delta\varepsilon_2^e$ and an inelastic, crack component $\Delta\varepsilon_2^i$ so that

$$\Delta\varepsilon_2 = \Delta\varepsilon_2^e + \Delta\varepsilon_2^i \,. \tag{31}$$

For the elastic part we define

$$\Delta\sigma_2 = E\Delta\varepsilon_2^e \,, \tag{32}$$

and for the cracked part it is assumed that

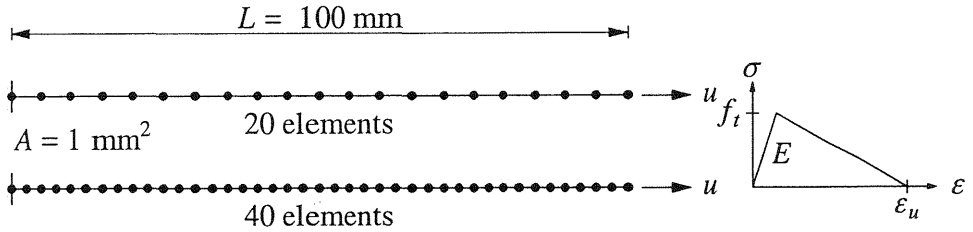

Fig. 3. Tension bar with truss elements.

$$\Delta\sigma_2 = h\,\Delta\varepsilon_2^i \,, \tag{33}$$

with h the softening modulus taken here as a constant equal to $h = -f_t/\varepsilon_u$, with f_t the tensile strength and ε_u the ultimate strain. If we substitute eq.(32) and (33) into (31) we obtain

$$\Delta\sigma_2 = \frac{hE}{h+E}\Delta\varepsilon_2 \,. \tag{34}$$

The expressions (30) and (34) can be used in eq.(29) which yields

$$E\Delta\varepsilon_1 = \left(E - \frac{E^2}{E+h}\right)\Delta\varepsilon_2 \,. \tag{35}$$

Combination of eq.(35) with (25), (26) and (28) gives an explicit expression for the amplitudes

$$\alpha_1 = \frac{(l/(d-l))E}{h + (E+h)(l/(d-l))} \tag{36}$$

and

$$\alpha_2 = \frac{E}{h + (E+h)(l/(d-l))} \,. \tag{37}$$

So, α_1 and α_2 are functions of softening modulus h. If we have nonlinear softening the mode amplitudes changes during local iterations for an accurate stress update. For the truss element the areas $\Omega_1 = (d-l)A$ and $\Omega_2 = l\,A$ in eqs.(22) and (24) with A the cross-section of the truss.

A tension bar modelled with truss elements (Figure 3) is analyzed with and without the inclusion of localized modes. Two different meshes have been used with 20 and 40 truss elements, respectively. The length of the bar $L = 100$ mm and the cross-section $A = 1$ mm^2. The material parameter set is as follows : the Young's modulus $E = 10.000$ N/mm^2, the tensile strength $f_t = 1$ N/mm^2 and the ultimate strain $\varepsilon_u = 0.01$. One element at the left boundary is given a small material imperfection. With standard elements without the additional mode (Figure 4-top-left) the results are mesh dependent. More elements produce a more brittle response. If we use a

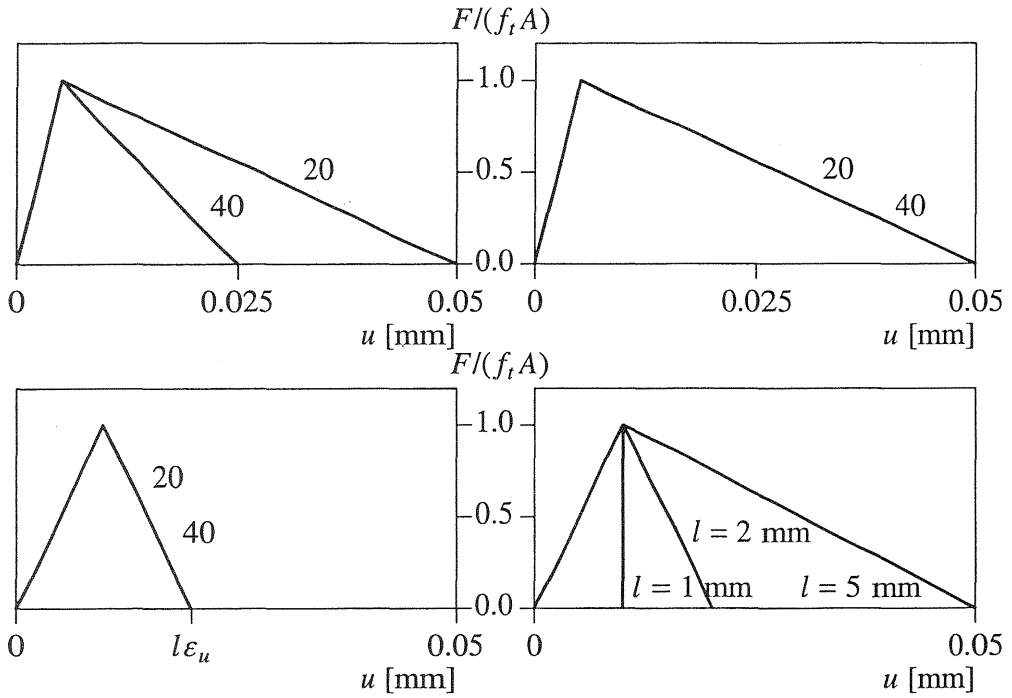

Fig. 4. Top-left: standard model. Top-right: fracture energy model. Bottom-left: embedded discontinuity model. Bottom-right: variation of l.

fracture energy model results can be made mesh independent (Figure 4-top-right). For this model the softening modulus is made a function of the element size (here $\sqrt{A}$, with A the area of a finite element) by taking $\varepsilon_u = 0.01$ for the 20 elements mesh and $\varepsilon_u = 0.02$ for the 40 elements mesh. Use of the embedded discontinuity elements with the localization band width $l = 2$ mm for the two analyses also solves the problem (Figure 4-bottom-left). Variation of l shows that the response is more brittle with $l = 1$ mm (vertical drop in load at peak load) and more ductile with $l = 5$ mm (Figure 4-bottom-right). In section 7 a comparison of the embedded crack model and the fracture energy model will be made.

5 2D element

For 2D analyses we use a constant strain triangular element to which the localized mode is added (see Figure 5). The jump in velocity gradient for the plane stress situation is (cf. eq.(2))

$$\begin{pmatrix} [\![\dot{\varepsilon}_{xx}]\!] \\ [\![\dot{\varepsilon}_{yy}]\!] \\ [\![\dot{\gamma}_{xy}]\!] \end{pmatrix} = \bar{\alpha} \begin{pmatrix} m_x \cos\theta \\ m_y \sin\theta \\ m_x \sin\theta + m_y \cos\theta \end{pmatrix} = \bar{\alpha}\mathbf{q} \,, \tag{38}$$

in which $(n_x, n_y)^{\mathrm{T}} = (\cos\theta, \sin\theta)^{\mathrm{T}}$. Similar to the 1D element a dual set of stresses $\boldsymbol{\sigma}_1$ and $\boldsymbol{\sigma}_2$ and strains $\boldsymbol{\varepsilon}_1$ and $\boldsymbol{\varepsilon}_2$ exist in the single integration point. For the elastic part we have

$$\dot{\boldsymbol{\sigma}}_1 = \mathbf{D}^e \dot{\boldsymbol{\varepsilon}}_1 \,, \tag{39}$$

and for the localized part we again assume a decomposition of total strain rate into elastic strain rate $\dot{\boldsymbol{\varepsilon}}^e$ and the crack strain rate $\dot{\boldsymbol{\varepsilon}}^i$

$$\dot{\boldsymbol{\varepsilon}}_2 = \dot{\boldsymbol{\varepsilon}}_2^e + \dot{\boldsymbol{\varepsilon}}_2^i \,. \tag{40}$$

To describe fracture the embedded discontinuity concept can be combined with the standard constitutive relations for fracture (fixed/rotating crack model) or plasticity (Rankine model).

5.1 Fixed/rotating crack concept

When incorporating crack stress - crack strain laws it is convenient to use the local n,t-coordinate system in a two-dimensional configuration, which is aligned with the discontinuity (see Figure 1). This necessitates a transformation between the crack strain rate $\dot{\boldsymbol{\varepsilon}}_2^i$ in the global x, y, z-coordinates and the crack strain rate $\dot{\mathbf{e}}_2^i$ in the local coordinates. The relation between local and global strain rates reads

$$\dot{\boldsymbol{\varepsilon}}_2^i = \mathbf{N}\dot{\mathbf{e}}_2^i \quad \text{with} \quad \dot{\mathbf{e}}_2^i = [\, \dot{e}_2^{nn} \,, 2\dot{e}_2^{nt} \,]^{\mathrm{T}} \,, \tag{41}$$

where $\dot{e}_2^{nn}$ is the mode-I crack normal strain rate, $\dot{e}_2^{nt}$ is the mode-II crack shear strain rate and $\mathbf{N}$ is the transformation matrix given by

$$\mathbf{N} = \begin{bmatrix} \cos^2\theta & -\sin\theta\cos\theta \\ \sin^2\theta & \sin\theta\cos\theta \\ 2\sin\theta\cos\theta & \cos^2\theta - \sin^2\theta \end{bmatrix} , \tag{42}$$

with θ the inclination angle of the normal of the crack $\mathbf{n}$ with the x-axis (see Figure 1). The angle is determined by the principal stress direction at the onset of cracking. An essential feature of the model is that $\mathbf{N}$ is fixed upon crack formation so that the concept belongs to the class of fixed crack concepts. If we let the discontinuity plane rotate with principal stresses a so-called rotating discontinuity model can be obtained.

The relation between the stress rate in the global coordinate system and the local stress rate can be derived to be

$$\dot{\mathbf{t}}_2 = \mathbf{N}^{\mathrm{T}}\dot{\boldsymbol{\sigma}}_2 \quad \text{with} \quad \dot{\mathbf{t}}_2 = [\, \dot{t}_2^{nn} \,, \dot{t}_2^{nt} \,]^{\mathrm{T}} \,, \tag{43}$$

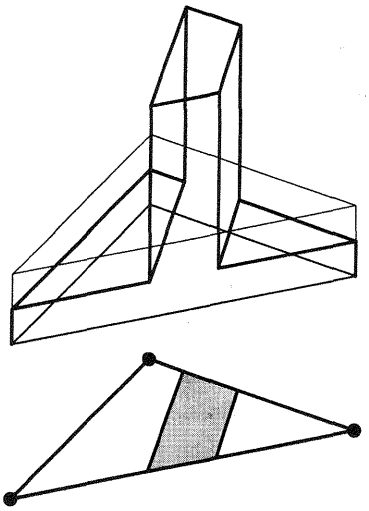

Fig. 5. Constant strain triangle with additional localized mode.

in which $\dot{t}_2^{nn}$ is the mode-I normal crack stress rate and $\dot{t}_2^{nt}$ is the mode-II shear crack stress rate. To complete the system of equations we need a constitutive model for the elastic contribution of the cracked material given by

$$\dot{\sigma}_2 = \mathbf{D}^e \dot{\varepsilon}_2^e \,, \tag{44}$$

and the relation between the local crack strain rate and the local crack stress rate

$$\dot{\mathbf{t}}_2 = \mathbf{D}^i \dot{\mathbf{e}}_2^i \,. \tag{45}$$

with

$$\mathbf{D}^i = \begin{bmatrix} h & 0 \\ 0 & \beta\mu \end{bmatrix}, \tag{46}$$

in which h is the mode-I softening modulus ($h<0$). The shear stiffness in the crack is obtained by a multiplication of the elastic shear stiffness μ with a shear reduction factor β. Coupling effects between the two modes are not considered. In this model fracture is assumed to be initiated in mode-I and mode-II effects enter upon rotation of the principal stresses. Combination of eqs.(39)-(46) gives the total stress-strain relation.

In the model the unknowns m_x, m_y, α_1 and α_2 need to be determined. Again, the assumptions of compatibility of deformation and traction continuity over the discontinuity lines have been used. Compatibility of deformation is assumed by means of

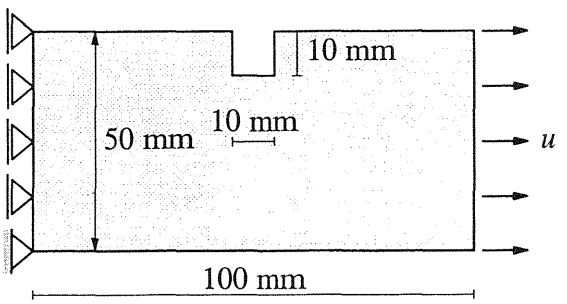

Fig. 6. Tension test on single-notched specimen.

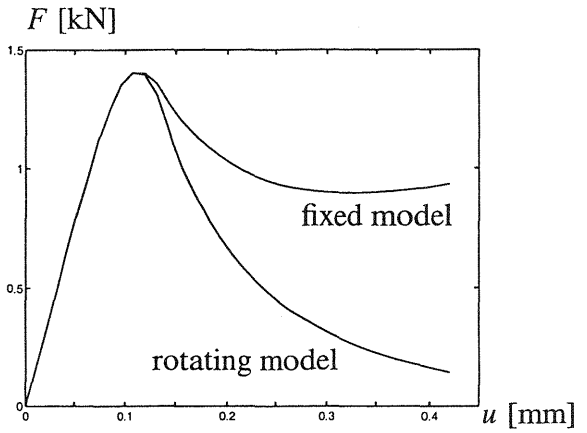

Fig. 7. Stress locking - fixed *versus* rotating concept.

$$\int_{\Omega} \dot{\boldsymbol{\varepsilon}}\, \mathrm{d}\Omega = \int_{\Omega_1} \dot{\boldsymbol{\varepsilon}}_1\, \mathrm{d}\Omega_1 + \int_{\Omega_2} \dot{\boldsymbol{\varepsilon}}_2\, \mathrm{d}\Omega_2 \,, \tag{47}$$

in which the total area of an element $\Omega = \Omega_1 + \Omega_2$ and $\dot{\boldsymbol{\varepsilon}} = \mathbf{B}\dot{\mathbf{a}}$ is the strain rate of the underlying element without additional modes. This condition coincides with a restriction that follows from the patch test, namely additional displacements due to extra nonconforming modes must vanish (Taylor et al., 1986). Furthermore, we assume traction continuity in a direction perpendicular to the discontinuity. So, if we consider the local n,t-coordinate system we assume that

$$\begin{pmatrix} [\![\dot{t}^{nn}]\!] \\ [\![\dot{t}^{nt}]\!] \end{pmatrix} = \mathbf{0} \,. \tag{48}$$

A complete calculation of the mode amplitudes is given by Sluys and Berends (1998).

A 2D tension test on a single-notched specimen is analyzed with the embedded discontinuity model. The problem is sketched in Figure 6. The material parameter set is taken from Berends et al. (1997) with exponential softening : $\sigma_{nn} = f_t \exp(-c e^i_{nn})$, with $c = 8.0$ and the localization band width $l = 1.0$ mm. A structured mesh is used with a single row of finite elements located verticallly under the notch. If we use the fixed concept we observe stress locking due to rotation of the stresses and a spurious build up of shear stress along the crack (dependent on the shear reduction factor β). If we let the discontinuity rotate with the principal stresses this shear stress cannot occur and the crack fully opens at zero stress (see Figure 7).

5.2 Rankine plasticity concept

Similarly a plasticity model can be used for the localized part of the element. As in the crack models the stress-strain relation can be written as

$$\dot{\sigma}_2 = \mathbf{D}^e(\dot{\varepsilon}_2 - \dot{\varepsilon}^i_2) \ . \tag{49}$$

For associative plasticity the plastic strain rate vector is defined as

$$\dot{\varepsilon}^i_2 = \dot{\lambda}\bar{\mathbf{n}} \ , \tag{50}$$

in which $\dot{\lambda}$ is a non-negative scalar and $\bar{\mathbf{n}}$ a vector, representing the magnitude and the direction of the plastic flow, respectively. The vector $\bar{\mathbf{n}}$ is taken as the normal to the yield surface f according to

$$\bar{\mathbf{n}} = \frac{\partial f}{\partial \sigma_2} \ . \tag{51}$$

The yield function f is a function of stress and the scalar-valued hardening/softening parameter κ. Rankine plasticity is defined as

$$f(\sigma_2, \kappa) = \sigma_i - h\kappa \ , i = 1, 2 \tag{52}$$

where σ_i are the two principal stresses. For plastic behavior we define

$$f(\sigma_2, \kappa) = 0 \quad \text{and} \quad \dot{f}(\sigma_2, \kappa) = 0 \tag{53}$$

with the second condition known as the consistency condition.

The angle θ follows from the major principal stress directions. Again, if we fix the direction upon initiation of the crack we have a fixed discontinuity model. On the other hand, if we let θ rotate after initiation we have a rotating discontinuity model. Again, the jump coefficients $\bar{\alpha}_1$ and $\bar{\alpha}_2$ in eqs.(7) and (8) are obtained from the compatibility condition and the assumption of stress continuity over the discontinuity line.

Now, the problem from Figure 6 is analyzed with the Rankine plasticity discontinuity model. The influence of the mesh configuration is studied. Three different unstructured meshes have been used with 147 (mesh 1), 301 (mesh 2) and 748 (mesh 3) elements, respectively, to investigate crack propagation. The material parameter set is as follows : the Young's modu-

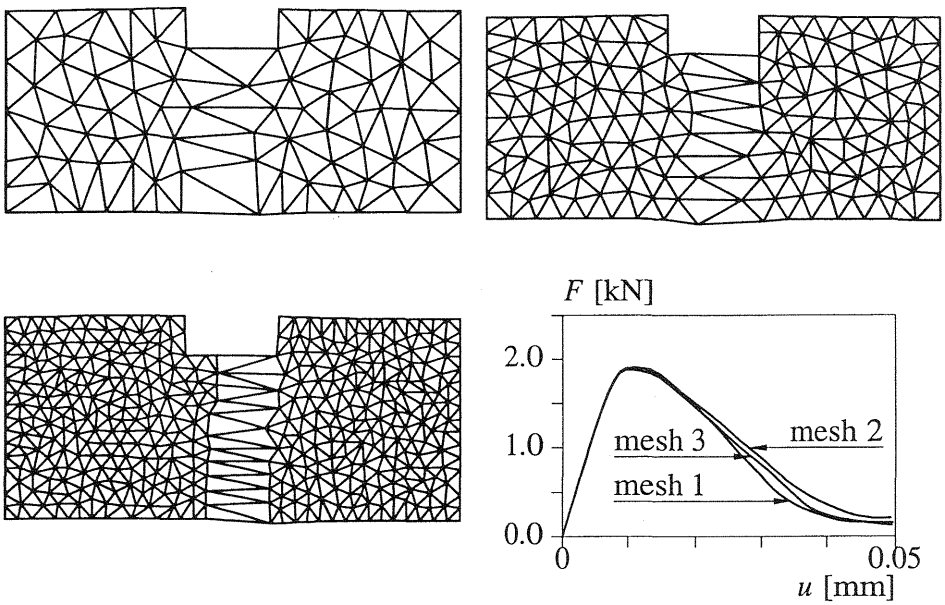

Fig. 8. Deformed model at $u = 0.05$ mm and load-displacement diagram.

lus $E = 10000$ N/mm^2, Poisson's ratio $\nu = 0.2$, the tensile strength $f_t = 1$ N/mm^2, the ultimate strain $\varepsilon_u = 0.015$ (linear softening) and the localization band width $l = 2$ mm. No stress locking occurs with the plasticity model combined with the fixed discontinuity concept. In the three unstructured meshes the proper crack path is found and the results are not dependent on the mesh size as can be seen from the deformed models and load-displacement curve in Figure 8.

6 3D element

For the 3D analyses 4-noded tetrahedron elements have been used. Again, a single integration point with a dual set of strains and stresses is assumed. Now we define the jump in strains with respect to the local n, t, s-basis. Eq.(2) then transforms in

$$([\![\dot{e}_{nn}]\!], [\![\dot{e}_{tt}]\!], [\![\dot{e}_{ss}]\!], [\![\dot{e}_{nt}]\!], [\![\dot{e}_{ts}]\!], [\![\dot{e}_{sn}]\!])^{\mathrm{T}} = \bar{\alpha}(m_n, 0, 0, m_t, 0, m_s)^{\mathrm{T}} = \bar{\alpha}\mathbf{q} \quad (54)$$

with

$$m_n^2 + m_t^2 + m_s^2 = 1\,. \quad (55)$$

The same derivation as for the 2D element is followed. For the fracture model the relation between the local crack strain rate ($[\dot{e}_2^{nn}, \dot{e}_2^{nt}, \dot{e}_2^{ns}]$) and the local stress rate ($[\dot{t}_2^{nn}, \dot{t}_2^{nt}, \dot{t}_2^{ns}]$) is given by

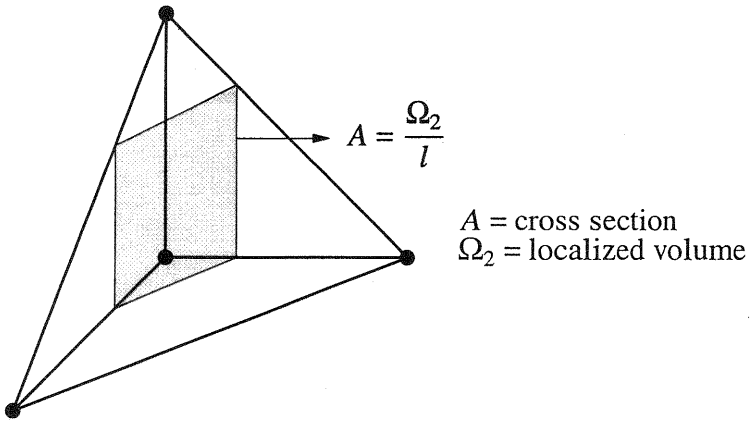

Fig. 9. Discontinuity plane in 3D element.

$$\dot{\mathbf{t}}_2 = \mathbf{D}^i \dot{\mathbf{e}}_2^i \ . \tag{56}$$

with $\mathbf{D}^i = diag[h, \beta\mu, \beta\mu]$. For Rankine plasticity we define

$$f(\sigma_2, \kappa) = \sigma_i - h\kappa \ , i = 1 \text{ to } 3 \tag{57}$$

where σ_i are the three principal stresses.

The compatibility assumption results in

$$\bar{\alpha}_1 = c\bar{\alpha}_2 \quad \text{with} \quad c = \frac{\Omega_2}{\Omega_1} \ , \tag{58}$$

in which Ω_1 and Ω_2 are volumes set by the orientation of the plane in the tetrahedron and the length scale parameter (see Figure 9). With the traction continuity condition

$$\begin{pmatrix} [\![\dot{t}^{nn}]\!] \\ [\![\dot{t}^{nt}]\!] \\ [\![\dot{t}^{ns}]\!] \end{pmatrix} = \mathbf{0} \ , \tag{59}$$

we complete the set of equations.

The single-notched specimen is now analyzed in a full 3D set-up. The specimen has a thickness of 50 mm and all parameters are as described in section 5.2. Three structured meshes have been used with 210 (mesh 1), 1100 (mesh 2) and 9800 (mesh 3) elements, respectively. The meshes consist of cubes which are patches of 5 tetrahedrons. Only mesh 3 has two vertical rows of elements under the notch. For this mesh a small material imperfection in one cube (5 tetrahedrons) is applied to trigger crack initiation at one side of the notch. The Rankine plasticity model is used with the fixed discontinuity concept. Figure 10 shows the nonuniform opening of the crack. Just after initiation of the crack a significant bending effect can

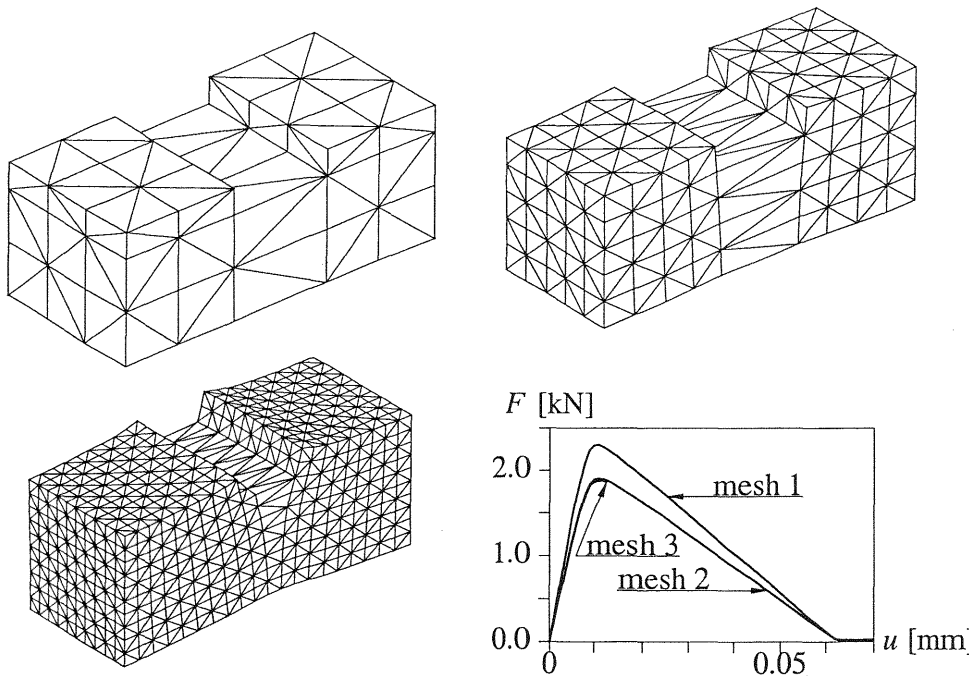

Fig. 10. Deformed models at $u = 0.06$ mm (mesh 1), $u = 0.03$ mm (mesh 2) and $u = 0.012$ mm (mesh 3) and load-displacement diagram.

be observed (see mesh 3 at $u = 0.012$ mm). Then the crack forms over the height of the specimen (see mesh 2 at $u = 0.03$ mm) and finally the crack fully opens and the deformation pattern becomes symmetric (see mesh 1 at $u = 0.06$ mm). An indirect displacement control technique is used to calculate the post-peak response. From the load-displacement curve it is clear that mesh 1 is far too coarse. Therefore a small locking effect in the elastic range (stiffness and limit load are too high) occurs. Mesh 2 and 3 are fine enough but it should be said that convergence problems avoid the calculation of the complete post-peak branch for the finest mesh.

7 Comparison with fracture energy type model

The embedded crack or embedded discontinuity model can be compared with the so-called fracture energy model or crack band model (Pietruszczak and Mróz, 1981; Bažant and Oh, 1983; Rots, 1988). In this model the crack is smeared over the finite element and the softening modulus is made a function of the finite element size. It can be shown that the embedded crack model provides exactly the same set of discretized equations as for the fracture energy model in the one-dimensional case under a pure mode-I loading and with the length scale in the embedded crack model taken equal

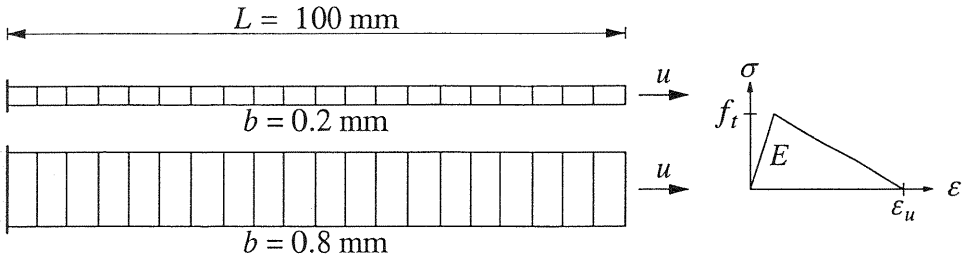

Fig. 11. Tension bar with different height b (20 elements).

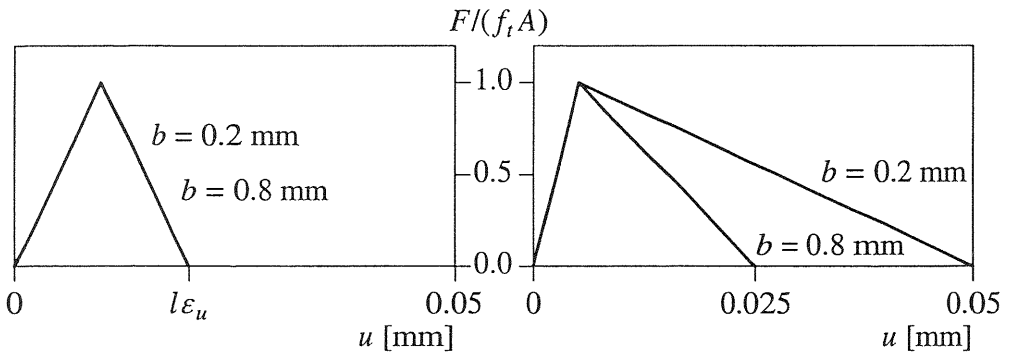

Fig. 12. Left: embedded crack model. Right: fracture energy model.

to the element size (see Figure 4 top-right and Figure 4 bottom-left, with l = 5 mm the two pictures are identical). In general, the formulations are different and a first advantage of the embedded model is that the length scale parameter l acts as a material parameter and is not dependent on the finite elemtent size. Secondly, the orientation of the crack is taken into account in the embedded crack model and not in the fracture energy model. This can be demonstrated by means of the example from Figure 11. A thickness increase in the direction of the crack should not affect the stress-displacement curve. However, if we take the crack band width in the fracture energy model w equal to $\sqrt{A}$ with A the area of a finite element (for 20 elements and height b = 0.2 mm : w = 1 mm $\rightarrow$ $\varepsilon_u = 0.01$ and for 20 elements and height b = 0.8 mm : w = 2 mm $\rightarrow$ $\varepsilon_u = 0.005$) we see a clear impact of the height increase on the stress-displacement curve (Figure 12-right) which is not present for the embedded crack model with l = 2 mm (Figure 12-left). Thirdly, with the embedded crack model a secondary mesh-sensitivity effect of the shear component is solved. Namely, in the fracture energy model the shear reduction factor β is a constant and not a function of the element size (Note that the definition of β in Figure 13 is slightly different from the definition in eq.(46) and eq.(57), because it sets the total shear stress - shear strain relation). As a consequence, the use of a

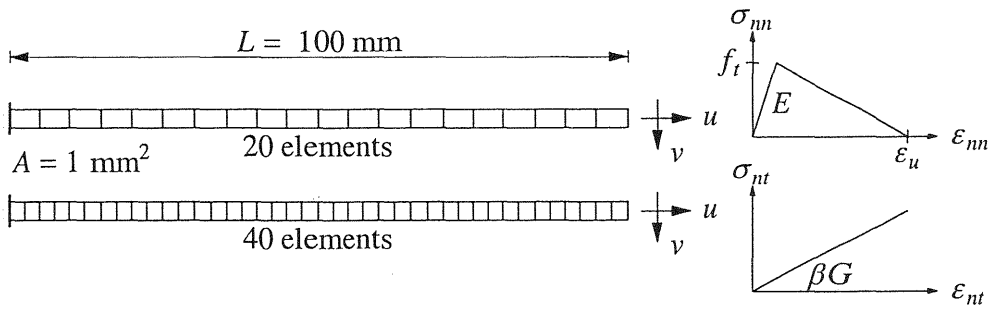

Fig. 13. Tension bar under combined tension/shear.

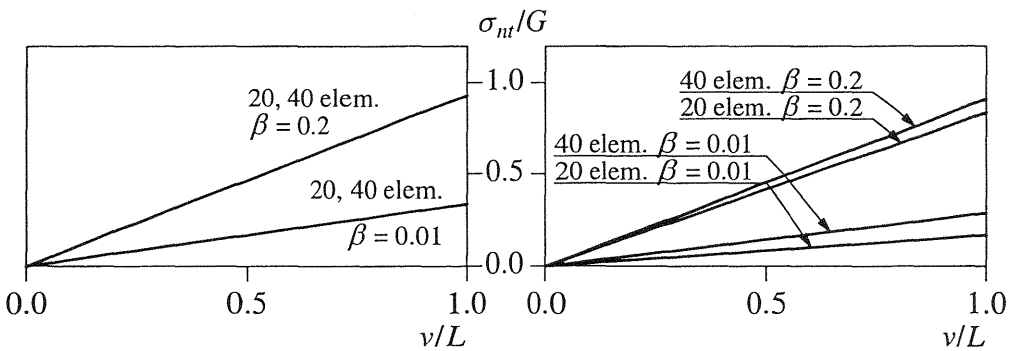

Fig. 14. Left: embedded crack model. Right: fracture energy model.

finer mesh leads to a smaller cracked area in which the shear stiffness is reduced and to mesh dependence. On the other hand, in the embedded crack model the area in which the shear stiffness is reduced is set by l and is not a function of the element size. In Figure 13 and 14 this mesh sensitivity effect is demonstrated. In the example the bar is loaded in tension until a crack occurs in the imperfect element. Then a shear deformation is applied while all further horizontal displacements are prevented to exclude bending effects in the bar (and crack closure in the imperfect element). When β is increased the effect vanishes (if $\beta = 1.0$ there is no effect). This example explains why the use of the fracture energy model with very fine meshes shows more stress locking than with coarse meshes (when a fixed smeared crack concept is used). In the embedded discontinuity model stress locking still exists (see Figure 7), but it is not dependent on the element size.

8 References

Aifantis, E.C. (1984). On the microstructural origin of certain inelastic models. **J. Engng Mater. Technol.,** 106, 326-334.

Armero, F. and Garikipati, K. (1995). Recent advances in the analysis and numerical simulation of strain localization in inelastic solids, **Computational Plasticity, Fundamentals and Applications,** (eds. D.R.J. Owen and E. Oñate), 547-561, Pineridge Press, Swansea.

Bažant, Z.P. and Oh, B. (1983). Crack band theory for fracture of concrete. **Mat. and Struct.,** 16, 155-177.

Belytschko T., Fish J. and Engelman B.E. (1988). A finite element with embedded localization zones. **Comp. Meth. Appl. Mech. Engng,** 70, 59-89.

Berends, A.H., Sluys, L.J. and Borst, R. de (1997). Discontinuous modelling of mode-I failure, **Finite Elements in Engineering Science,** (eds. M.A.N. Hendriks, H. Jongedijk, J.G. Rots and W.J.E. van Spanje). 351-361, Balkema, Rotterdam.

Borst, R. de, Sluys, L.J., Mühlhaus, H.-B. and Pamin, J. (1993). Fundamental issues in finite element analyses of localization of deformation. **Engng Comput.,** 10, 99-121

Larsson R., Runesson K. and Akesson M. (1995). Embedded localization based on regularized strong discontinuity, **Computational Plasticity, Fundamentals and Applications,** (eds. D.R.J. Owen and E. Oñate), 599-610, Pineridge Press, Swansea.

Lotfi, H.R. and Shing, P.B. (1995). Embedded representation of fracture in concrete with mixed finite elements. **Int. J. Num. Meth. Engng,** 38, 1307-1325.

Ortiz, M., Leroy, Y. and Needleman, A. (1987). A finite element method for localized failure analysis. **Comp. Meth. Appl. Mech. Engng,** 61, 189-214.

Pietruszczak, S. and Mróz, Z. (1981). Finite element analysis of deformation of strain softening materials. **Int. J. Num. Meth. Engng,** 17, 327-334.

Pijaudier-Cabot, G. and Bažant, Z.P. (1987). Nonlocal damage theory. **ASCE J. Eng. Mech.,** 113, 1512-1533.

Rots, J.G. (1988). **Computational modeling of concrete fracture,** Dissertation, Delft University of Technology, Delft.

Simo, J.C., Oliver, J. and Armero, F. (1993). An analysis of strong discontinuities induced by softening solutions in rate-independent solids. **J. Comput. Mech.,** 12, 277-296.

Sluys, L.J. and Berends, A.H. (1998). Discontinuous failure analysis for mode-I and mode-II localization problems. **Int. J. Solids Structures,** accepted for publication.

Taylor, R.L., Simo, J.C., Zienkiewicz, O.C. and Chan, A.C.H. (1986). The patch test - A condition for assessing FEM convergence. **Int. J. Num. Meth. Engng,** 22, 39-62.